AN EMPIRICAL STUDY OF RELATIONSHIPS BETWEEN URBAN LIGHTING INDICATORS AND NIGHT-TIME LIGHT RADIANCE

F. Kekula, P. Hrubeš**

Abstract: Night-time light (NTL) radiance has a great potential in analyses of dynamic changes in patterns of human activities, and socio-economic and demographic factors. However, most of those analyses are focused on factors at global scales such as the population size, gross domestic product, electric power consumption, fossil fuel carbon dioxide emission etc. In this study we investigate the relationships between three urban lighting indicators and monthly averaged NTL radiance obtained from NASA's Black Marble monthly NTL composites for 4 study areas in the Czech Republic at local scale. The Pearson correlation analysis was used to identify a strength of the correlations between the indicators and radiance at near-nadir for two different snow conditions. The results from the correlation show that radiance has a strong positive correlation with the number of street-lighting points and their total nominal power, while for the average mast height there were observed moderate correlation coefficients. However, the areas with larger scales have higher correlation coefficients. Moreover, we found that the correlation coefficients are higher for snow-covered condition radiances. Generalized linear (GL) regression analysis was used to examine an association between the radiance and selected indicators. Owing to the excess zeros and overdispersion in the data, the zero-inflated regression performs better than the GL regression. Results from the regression analysis evince a statistically significant relationship between the radiance and selected indicators.

Key words: *night-time lights radiance, urban lighting indicators, Pearson correlation coefficient, generalized linear model, zero-inflated Poisson model*

Received: September 1, 2023
Revised and accepted: October 22, 2023

DOI: 10.14311/NNW.2023.33.021

1. Introduction

Urban lighting planning represents a key element for ensuring sufficient illumination in order to improve environment perception and facilitate orientation, safety and security during low lighting levels or adverse weather conditions [26] by means of urban lighting installations. There have been published several studies revealing

*František Kekula – Corresponding author; Pavel Hrubeš; Czech Technical University in Prague, Faculty of Transportation Sciences, Konviktská 20, CZ-110 00 Praha 1, Czech Republic, E-mail: kekulfra@fd.cvut.cz, hrubes@k620.fd.cvut.cz

that the appropriate urban lighting installations can improve not only the perception of space and pedestrians' mobility behaviour in cities and municipalities when darkness falls [33, 1, 34, 29, 9, 15]. However, they can also have impact on road safety [13, 3, 46, 21, 35, 23].

Every part of a city has its own functional utilization which should always be in accordance with a given urban lighting that can be differentiate to the utility lighting and architectural lighting [26]. The urban lighting installations differ in technical lighting parameters, construction and design solutions, geometrical arrangements, and geographical locations creating a complicated heterogeneity of spatial patterns of the illumination characteristics across different land uses, such as main roads, commercial and institutional areas, residential areas etc. NTL imagery provides a powerful geospatial resource to detect low radiance at night, and thus it is able to perceive dynamic changes of the world in human activities and environmental changes, locally and globally [52] through the measure of the radiance from space. NTL data have been extensively used in mapping urban areas [41, 47, 18] and in estimating socio-economic factors such as population changes [51, 2], gross domestic product [6, 19], income [20], electric power consumption [5], and freight traffic [42]. Some studies have also been concerned with mapping of conflicts and disasters and environmental changes such as fisheries [43, 17], and light pollution [24].

However, most of these studies investigating the relationships between NTL radiances and human-linked patterns were performed at macro scales. The NTL data used in these studies were mainly collected from the Defense Meteorological Satellite Program's Operational Linescan System (DMSP–OLS). Nevertheless, this data suffer, among others shortcomings, mainly from coarse spatial resolution, lack of on-board calibration, and signal saturation in bright urban core areas (radiometric resolution of six bits) [11, 27]. The major challenge is the lack of a finer spatial resolution to record the detailed spatial and temporal patterns of the NTL radiances at local scales. NASA's Black Marble NTLs product suite represents the new generation of the NTL data that has a vast improvement in spatial resolution over DMSP-OLS, and thus offers more detailed characterization of natural and artificial spatial patterns of light that escape to space.

This paper is aimed at the investigation of the relationship between the NTL radiance and three selected urban lighting indicators within 4 urban study areas in the Czech Republic. The urban lighting indicators we chose in this study are the number of street-lighting points (NSLPs), total nominal power of street-lighting points (TNPSLPs), and average mast height of street-lighting points (AMHSLPs). The correlation analysis was used to identify the most promising indicators suitable for use in the subsequent regression analysis. It is hypothesized that the NTL data could be a good proxy for some of the above-mentioned indicators.

The rest of the paper is structured as follows. In Section 2, employed data in the investigation process are described, including the NTL data, and ancillary GIS data. In Section 3, the data pre-processing steps and statistical analysis are explained. In Section 4, the results of the correlation and regression analyses are summarized. In Section 5, the main conclusions of this paper are presented.

2. Study areas and datasets

In this study we incorporate both satellite imagery, and spatial GIS layers intended for the study areas in the Czech Republic. Detailed description of the study areas and used datasets will be presented in the following sub-sections.

2.1 Study areas

The considered study areas are located in the Czech Republic representing two cities (study areas 1 and 3), one town (study area 2), and one village (study area 4) with different urban forms and population sizes. The principle of the selection was to include the areas with different geographic and demographic characteristics so as to make sample more representative. These areas were used in the investigation of the relationship between the NTL radiance and the urban lighting indicators. Geographical locations of the study areas within the Czech Republic with their names can be seen in Fig. 1.

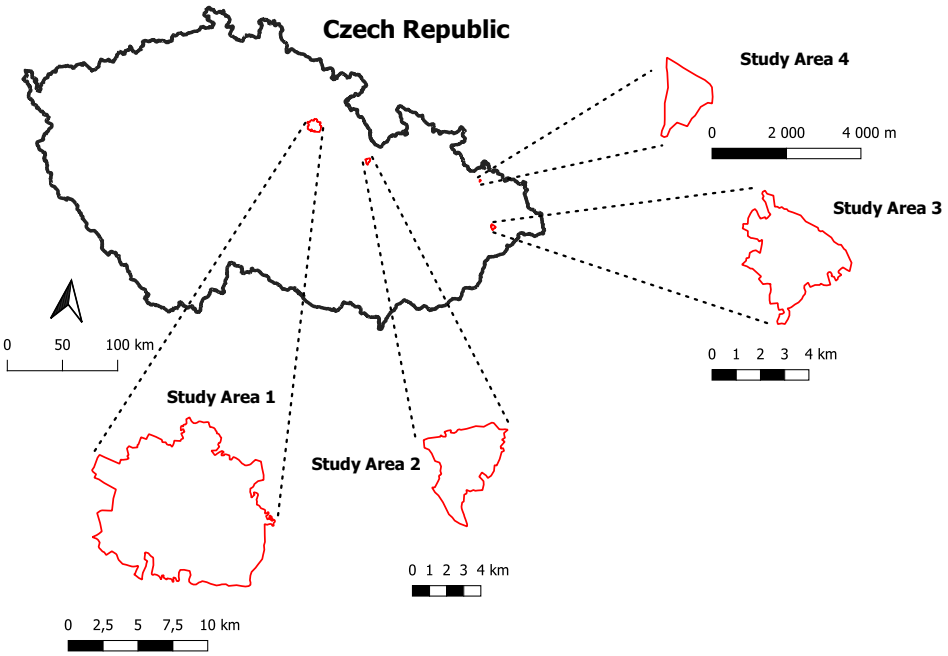

Fig. 1 *Location of the study areas in the Czech Republic. The considered study areas are represented by the red polygons (Study Area 1 – Hradec Králové, Study Area 2 – Dolní Čermná, Study Area – Frenštát pod Radhoštěm, Study Area 4 – Nové Sedlice).*

2.2 Datasets

2.2.1 Night-time lights imagery

The NTL data from the NASA's Black Marble night-time lights product suite (VNP46; [38]) at 15 arc-second spatial resolution (around 500 m) is used for investigating of the relationships between the NTL radiance and urban lighting indicators. The NTL product suite can be created owing to the Visible Infrared Imaging Radiometer Suite (VIIRS) sensor onboard the Environmental Satellite System Suomi National Polar Partnership (NPP) [32], launched in October 2011. This satellite is equipped with a specific panchromatic sensor which is designed for measuring (or sensing) night-time lights – the Day and Night Band (DNB) [31]. It represents a significant improvement in terms of data availability and observing characteristics over DMSP–OLS [12], the previous system for collecting NTLs.

The NASA's Black Marble products suite consists of four products, such as top-of-atmosphere (TOA) DNB radiance along with ancillary data (VNP46A1; [38]), lunar BRDF-corrected radiance (VNP46A2; [38]), monthly composite radiance (VNP46A3; [38]) and annual composite radiance (VNP46A4; [38]) [44]. For the purpose of this study we used the VNP46A3 product including 28 scientific datasets (layers) with the information on the NTL composites, the number of observations, quality, and standard deviation for multi-view zenith angle categories (near-nadir, off-nadir, and all angles) and snow status (snow-covered and snow-free), land water mask, platform, latitude, and longitude [37]. The monthly NTL composites were generated from moon-free and moon-lit atmospherically and lunar-BRDF-corrected NTL from the product VNP46A2 [45]. All scientific datasets store the data in the standard land Hierarchical Data Format-Earth Observing System (HDF–EOS) format [37]. Appropriate HDF–EOS files were downloaded from the data centre of NASA's Level-1 and Atmosphere Archive and Distribution System (LAADS) Distributed Active Archive Centers (DAACs) through its web interface (https://ladsweb.modaps.eosdis.nasa.gov/).

2.2.2 Ancillary open GIS data

Data on the urban lighting installations were downloaded in comma-separated values files through geo-portals as open data administrated by a given city or municipality. These files contain several attributes which characterize a given lighting installation. From this set of attributes we chose only three attributes called the urban lighting indicators: the NSLPs, (TNPSLPs), and (AMHSLPs). To separate administrative regions of study areas we used the Data200 database (downloaded from the link Data200) which represents a digital geographic model of the territory of the Czech Republic and it is managed by the Czech Office for Surveying, Mapping and Cadastre (ČÚZK). From this database we used only the polygon vector layers represent the administrative borders of the study areas.

3. Methodology

3.1 Imagery preprocessing

3.1.1 Converting, mosaicking, re-projecting, and clipping

From the downloaded HDF5 files of the VNP46A3 product for the area of the Czech Republic the NTL temporal radiance composites were used and further pre-processed. The datasets of NTL temporal radiance composites for view zenith angle of category near-nadir and two different snow conditions (snow-free and snow-covered) were exported as raster layers in the GeoTiff file format. The exported layers had a coordinate system of WGS 84. The study areas are placed in the region of the Czech Republic which is covered by two tiles, namely the h19v03 and h19v04 tiles from the Suomi-NPP VIIRS linear latitude/longitude tile grid. These tiles were then mosaicked and re-projected to S–JTSK/Krovak Easth North coordinate system using gdal warp command utilities. Finally, we performed raster clipping in order to obtain the final raster composites for all study areas. All the mentioned raster operations are performed with the use of Geospatial Data Abstraction Library (GDAL) and its Python wrappers. Fig. 2 shows the steps of this procedure.

3.1.2 Spatio-temporal gap-filling of night-time lights radiance

Remote sensing data often contains low-quality or missing pixel values across the image scene that they cover [16]. In chosen data product VNP46A3 from the NASA's Black Marble product suite there are certain pixel positions with no data (or gaps), especially during winter or summer solstices. These gaps are mainly caused either by cloud contamination or solar illumination in summer [7, 53, 44]. In the case of selected study areas these gaps exist in the original January, February, March, May, June, July, and December VIIRS DNB composites with the most serious missing values in the May, and July composites and almost all missing values in the June. Therefore, this month was excluded from the analysis. To deal with this issue in remaining months we used the spatio-temporal prediction method proposed by [16] which predict missing values through quantile regression and its prediction algorithm is described elsewhere [16]. In our prediction procedure, we assumed that for each study area the selected urban lighting indicators remained unchanged from the time in which the urban lighting masterplan was created to 1 year onwards.

Our procedure for filling in missing data is outlined below:

1. **Subset selection:** For each study area, we determined the year and month of urban lighting masterplan creation. From that time-stamp a 1 year onwards we selected the VIIRS DNB monthly composites for both snow conditions and stacked them sequentially into 2 separate 12-month time series. Therefore, each pixel has 12 time series radiance values for two different snow conditions. In that original time series we identified radiance composites in which more than 50% pixels [16] have no data and excluded them from further steps of the procedure. In that case all the radiance composites for the June were

excluded. Thus, the final two time series to fill missing values in have only 11 months.

2. **Gapfill algorithm application:** In the second step, we applied the gapfill algorithm on the snow-free and snow-covered time series. The gapfill algorithm fills the missing values based on neighbouring observations within a spatial and temporal window expressed in four dimensions (dim 1 (longitude), dim 2 (latitude), dim 3 (month of the year), dim 4 (year)).

   The selected datasets act as the neighbouring observations to fill the missing values in, comprises two individually rank-4 tensors of shape (n_x, n_y, n_s, n_a), where n_x and n_y are the spatial extents of the composites (images), n_s is the number of composites within a year, and n_a is the number of years. In our case, both selected datasets (for the snow-covered and snow-free conditions) have a different spatial extent (based on the study area size) of radiance values consist of 99 images with the $n_s = 11$ (11 months) and $n_a = 9$ (between the years 2013–2021). The prediction method predicts each missing value separately and its procedure includes four steps. In the first step, selecting sufficiently large spatio-temporal neighbourhood prediction set for the prediction of target missing value is performed. The selection is based on iteratively increasing the initial spatial extent of the neighbourhood until two criteria are fulfilled which are described in greater detail in [16]. In step 2, scoring sub-images in the spatio-temporal neighbourhood prediction set according to scoring procedure described in [16] is carried out. In the last two steps, the empirical quantile of the target missing value is estimated and quantile regression is applied to the observed values of the prediction set [16].

3.2 GIS data preprocessing

In this paper we also incorporate the spatial GIS layers of administrative boundaries representing the study areas and comma-separated values files including parameters about the urban-lighting installations for that areas. Administrative boundaries were obtained from the "Data200" database which is a digital geographic model of territory of the Czech Republic organised in 8 thematic layers and provided as open database [8]. The comma-separated values files were obtained from the city municipalities within an initiative of open data. Thematic layers of administrative boundaries were used to create rectangular grids with their horizontal and vertical spacing equal to a spatial resolution of the VIIRS DNB monthly composites in order to calculate radiance values for each grid. These grids were created in Quantum GIS (QGIS) using the native routines "Create grid" and "Clip". For these grids, radiance values were calculated from the spatio-temporal gap filled VIIRS DNB monthly composites using the native routine "Zonal statistics" which weights pixel contribution by the area of a given rectangle. After that we imported the comma-separated values files into QGIS and exported them as ESRI shapefile point layers. By using the expression functions from the "array" and "geometry" groups through the QGIS Field Calculator tool we calculated statistic for chosen urban lighting parameters per each rectangle within a given study area grid, namely for the NSLPs, TNPSLPs and AMHSLPs.

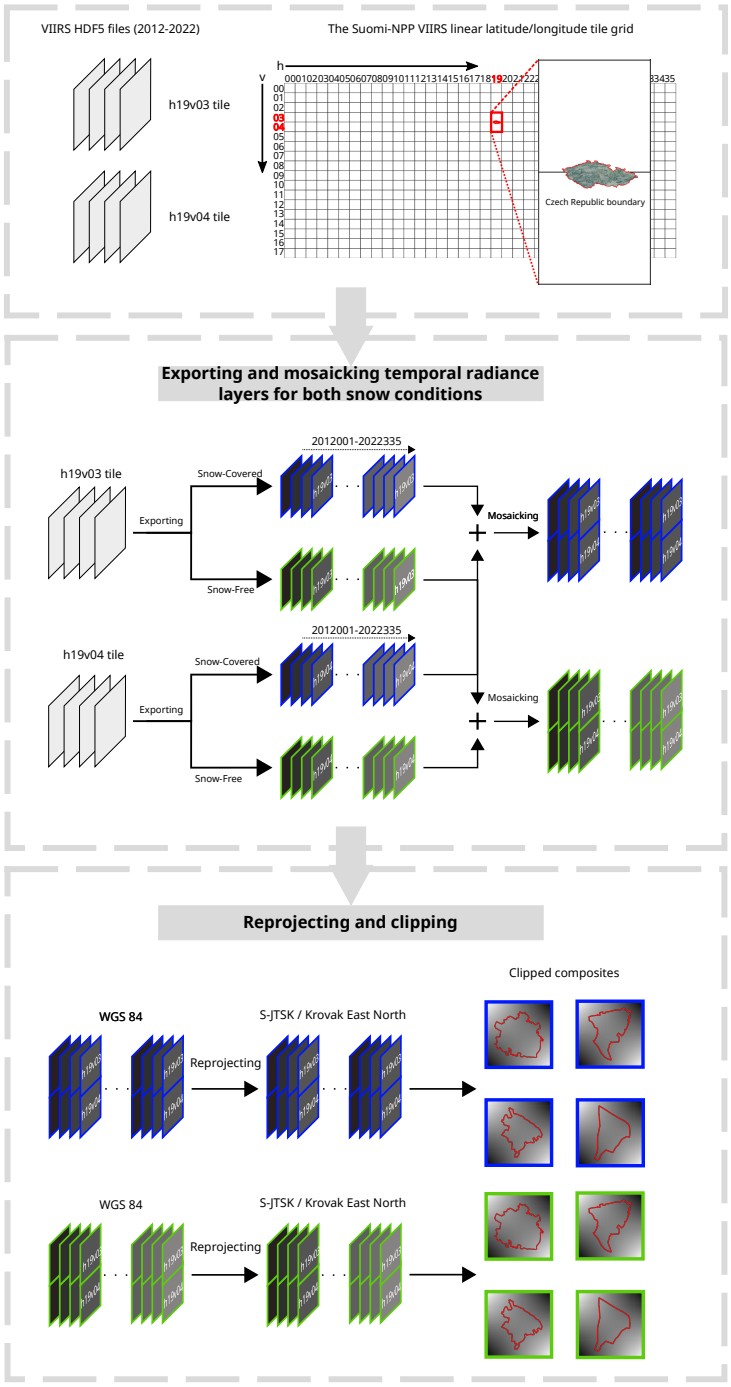

Fig. 2 *Procedure of NTL radiance composites preprocessing.*

3.3 Statistical analysis

3.3.1 Basic correlation

First, we examined the correlations between the NTL data and chosen urban lighting indicators for all study areas so as to identify bivariate relations between the radiance and indicators. We employed the radiances for both snow conditions in the correlations in order to be able to capture and examine possible differences. We assume that the most of the operational time of the urban-lighting installations is overlapping with the satellite overpass in the study areas. All variables used in the correlation analysis and their meanings are summarized in Tab. I.

Variable	Meaning of the variables
y_1	Number of street-lighting points (NSLPs)
y_2	Total nominal power of street-lighting points (TNPSLPs)
y_3	Average mast height of street-lighting points (AMHSLPs)
x	Monthly averaged radiance

Tab. I *All variables used in the correlation analysis.*

In order to measure the strength of the linear relationships between the indicators and the radiance, we computed sample Pearson correlation coefficients. 66 sample correlation coefficients were calculated for each study area, thus in total 264 sample correlation coefficients across all 4 study areas. We interpreted the high or strong correlations as correlations with the correlation coefficient above the value of 0.5, since these correlation values indicate that a variable tend to be good for modelling their linear relationship [14]. With the calculated sample correlation coefficients, the p-values were also determined providing the significances of the correlation coefficients. The p-values lower than 0.05 at 95% confidence level indicates statistically significant non-zero correlations. The analysis shows which correlations are statistically significant and which indicators correlate with the radiance. The results from the correlation analysis are presented in Fig. 3.

3.3.2 Simple regression analysis

In this section we introduce generalized linear (GL) regression and zero-inflated regression analyses in order to investigate the relationships between the radiance and indicators, thus ascertain the causal effect of the radiance upon the indicators. In other words, the indicators represent the response variables, and the radiance represents the explanatory variable. We note that in the regression analysis we used the radiance values for both snow conditions and for 4 months, such as the January, April, July, and October, as we suppose that these months are the most representative during a year. Tab. II shows the descriptive statistics of the response variables and Fig. 4 shows their respective histograms. Before the determination of the appropriate regression model, we performed the Poisson distribution testing on the response variables, such as the NSLPs and TNPSLPs in order to find out, whether or not the response variables are from the Poisson distribution. We chose

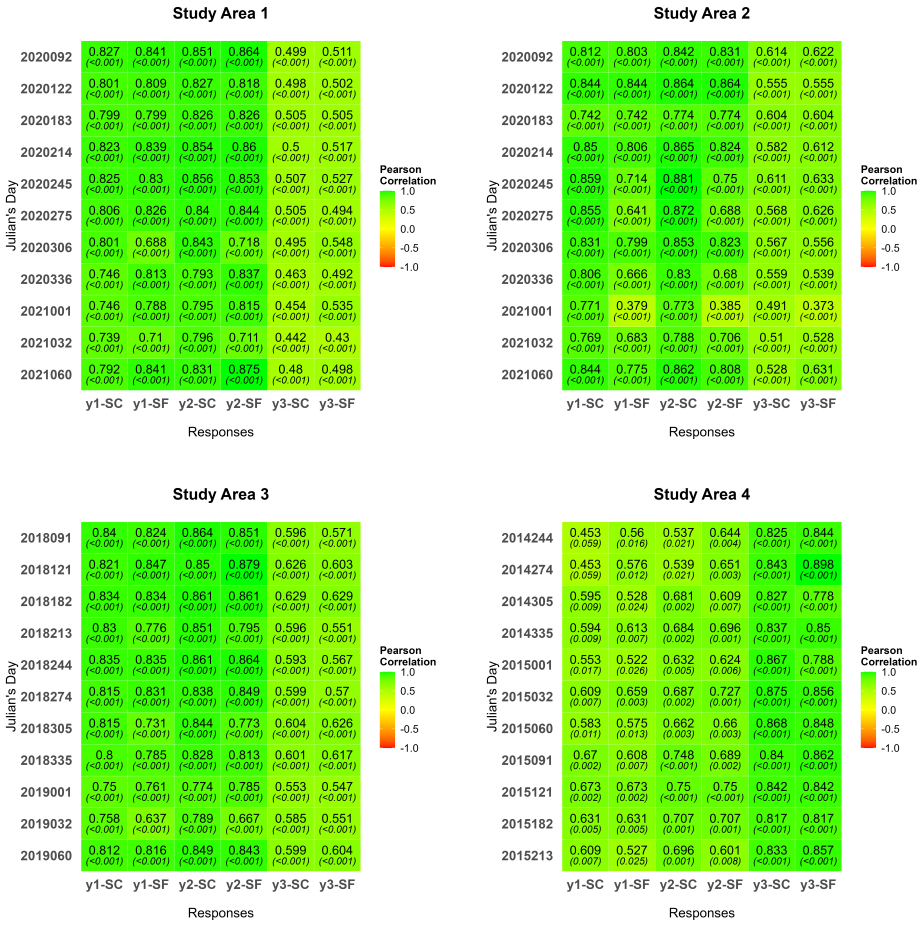

Fig. 3 *Sample correlation coefficients and their p-values for all study areas and all variables for both snow conditions (SC – snow covered, SF – snow free).*

Variable	Minimum	Maximum	Mean	Variance
y_1	0	581	20.424	2595.401
y_2	0	38622	1956.617	24358960.550

Tab. II *Descriptive statistics for chosen response variables y_1 and y_2.*

the Shapiro–Wilk's test over the Kolmogorov–Smirnov test due to its better performance even for small sample sizes [36]. The null and alternative hypotheses are as follows:

H_O: The response distribution is normal,

H_A: The response distribution is not normal.

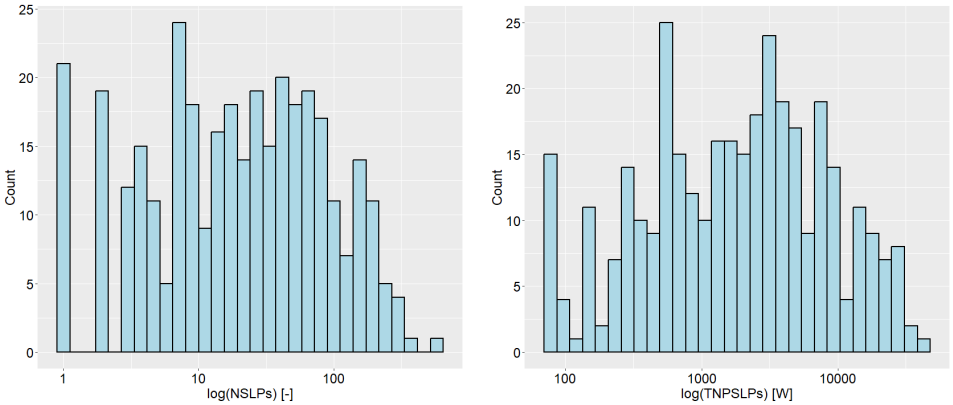

Fig. 4 *Histograms for both response variables (y_1 – left, y_2 – right).*

We computed a test statistic with the degree of confidence at 95%, or 0.05 significance. Results from computed test statistics for both responses are summarized in Tab. III. From the results we can reject the null hypothesis for both responses, since calculated p-values are less than 5% ($p < 0.05$), and thus implying that both responses are Poisson distributed. The presence of significant overdispersion in the data is apparent from Tab. II, where the variance values are much larger than the mean values. The Poisson regression model is based on the assumption that the response variable follows the probability mass function (PMF), which is usually given by [10]:

Variable	W	p-value
y_1	0.456606	< 0.001
y_2	0.453553	< 0.001

Tab. III *Results from Shapiro–Wilk normality tests for both response variables.*

$$\mathcal{P}(y_i;\mu_i) = \frac{e^{-\mu_i}\mu_i^{y_i}}{y_i!}, \quad y_i = 0,1,2,\ldots,n, \quad \mu_i > 0. \tag{1}$$

However, this PMF assume that the variance of Poisson randomly distributed variable equals its mean value so as to follow the expression $\mathrm{Var}(y_i) = \mathrm{E}(y_i)$. Therefore, we used the GL regression model in which the response variable y_i assumes the following form of PMF [49]:

$$\mathcal{P}(y_i;\mu_i,\delta) = \frac{\mu_i(\mu_i+\delta y_i)^{y_i-1}e^{-\mu_i-\delta y_i}}{y_i!}, \quad y_i = 0,1,2,\ldots,n, \quad \mu_i > 0, \tag{2}$$

where the δ is the dispersion parameter where its values lie in the interval $\max(-1, \frac{-\mu_i}{4}) < \delta < 1$. The mean and variance of the response variable y_i are given by the following formulae [22]:

$$\text{Mean}(y_i) = \frac{\mu_i}{1-\delta}, \tag{3}$$

$$\text{Var}(y_i) = \frac{\mu_i}{(1-\delta)^3}. \tag{4}$$

Afterwards, the GL model with one predictor was used with the following form with the random and systematic components defined as [10]:

$$\begin{cases} \text{Random component: } y_i \sim \mathcal{P}(y_i; \mu_i, \delta), \\ \text{Systematic component: } \log\mu_i = \beta_0 + \beta_1 x_i, \end{cases} \tag{5}$$

where the y_i is the response variable, log is the logarithmic link function, μ_i is the expected value of the response, x_i is the explanatory variable, and β_0 and β_1 are the regression parameters. The systematic component can be written as:

$$\mu_i = e^{\beta_0 + \beta_1 x_i}. \tag{6}$$

The results from the GL model for the response variables y_1 and y_2 are summarized in Tab. IV and Tab. V, respectively. The p-values of β_1 regression parameters are very low for both response variables across all 4 study areas and months even for both snow conditions. This could indicate that the NSLPs and TNPSLPs are strongly dependent on the radiance. However, the model evinces a significant overdispersion based on the calculated ratios of deviance to degrees of freedom ($\frac{\text{rd}}{\text{df}}$) which should be close to 1 as much as possible. It has a serious consequence on the trustworthiness of the test statistic as the variable will generally appear to be more significant that warranted by the data [10], and thus lead to misleading inference for the regression parameter. From the plotted histograms depicted in Tab. 4 it can be seen, that both variables have lot of zero values that can not be accounted only by the Poisson distribution [48]. Excessive amount of zero's values can cause extreme overdispersion in the model, and thus we used the zero-inflated Poisson (ZIP) model to adjust the model for this phenomena [25, 50]. The ZIP model comprises two regression portions, such as the logistic and Poisson regressions. The logistic regression predicts only the zero count due to excessive zeros, and Poisson regression predicts both the zero and non-zero counts [48]. Thus, the random component of the model comprises of two PMFs which are used to calculate the probability of observing a zero count and counts (including zeros) and are given by the following formulae [48]:

$$\mathcal{P}(y_i|x_i, z_i) = \begin{cases} p_i + (1-p_i)e^{-\mu_i}, & y_i = 0, \\ (1-p_i)\frac{e^{-\mu_i}\mu_i^{y_i}}{y_i!}, & y_i > 0, \end{cases} \tag{7}$$

where the μ_i is the Poisson mean, x_i represents the covariates for the logistic regression part, z_i represents the covariates for the Poisson regression part and p_i is the probability of extra zeros.

In the case in which the $p_i = 0$ the model is simplified to a regular Poisson model [39]. The results from the inflation and count portions for both response variables y_1 and y_2 are summarized in Tab. VI and Tab. VII, respectively. Both models were compared by calculation the likelihood measure of Akaike information

	Study Area 1				
Julians Date	β_1	p-value	$\frac{\text{rd}}{\text{df}}$	AIC	n
2021001 – SC	0.003	< 0.001	42.677	27291	608
2020092 – SC	0.004	< 0.001	30.892	20149	608
2020214 – SC	0.005	< 0.001	29.479	19293	608
2020306 – SC	0.004	< 0.001	35.354	22853	608
2021001 – SF	0.006	< 0.001	28.672	18804	608
2020092 – SF	0.004	< 0.001	26.760	17646	608
2020214 – SF	0.005	< 0.001	25.337	16783	608
2020306 – SF	0.007	< 0.001	37.411	24100	608
	Study Area 2				
Julians Date	β_1	p-value	$\frac{\text{rd}}{\text{df}}$	AIC	n
2021001 – SC	0.035	< 0.001	4.358	516	102
2020092 – SC	0.187	< 0.001	2.693	350	102
2020214 – SC	0.173	< 0.001	3.169	397	102
2020306 – SC	0.211	< 0.001	3.675	448	102
2021001 – SF	0.111	< 0.001	7.906	871	102
2020092 – SF	0.191	< 0.001	2.622	342	102
2020214 – SF	0.200	< 0.001	2.999	380	102
2020306 – SF	0.299	< 0.001	2.659	346	102
	Study Area 3				
Julians Date	β_1	p-value	$\frac{\text{rd}}{\text{df}}$	AIC	n
2019001 – SC	0.003	< 0.001	20.271	1790	84
2018091 – SC	0.016	< 0.001	9.021	868	84
2018213 – SC	0.019	< 0.001	9.444	902	84
2018305 – SC	0.017	< 0.001	10.104	956	84
2019001 – SF	0.014	< 0.001	15.729	1417	84
2018091 – SF	0.016	< 0.001	13.059	1198	84
2018213 – SF	0.019	< 0.001	14.744	1337	84
2018305 – SF	0.018	< 0.001	14.912	1350	84
	Study Area 4				
Julians Date	β_1	p-value	$\frac{\text{rd}}{\text{df}}$	AIC	n
2015001 – SC	0.054	< 0.001	7.381	150	18
2015091 – SC	0.070	< 0.001	5.524	120	18
2015213 – SC	0.070	< 0.001	6.478	135	18
2014305 – SC	0.047	< 0.001	7.248	148	18
2015001 – SF	0.046	< 0.001	8.062	161	18
2015091 – SF	0.094	< 0.001	6.208	131	18
2015213 – SF	0.057	< 0.001	7.966	159	18
2014305 – SF	0.042	< 0.001	8.216	163	18

Tab. IV *Results from the GL model for the response variable y_1 with different sample sizes 608, 102, 84, and 18 ($\frac{rd}{df}$ – ratio of deviance to degrees of freedom).*

	Study Area 1				
Julians Date	β_1	p-value	$\frac{\text{rd}}{\text{df}}$	AIC	n
2021001 – SC	0.003	< 0.001	3981.565	2415543	608
2020092 – SC	0.004	< 0.001	2930.363	1778514	608
2020214 – SC	0.005	< 0.001	2722.698	1652669	608
2020306 – SC	0.004	< 0.001	3260.585	1978629	608
2021001 – SF	0.006	< 0.001	2650.581	1608966	608
2020092 – SF	0.005	< 0.001	2511.066	1524420	608
2020214 – SF	0.005	< 0.001	2378.754	1444239	608
2020306 – SF	0.008	< 0.001	3497.650	2122290	608
	Study Area 2				
Julians Date	β_1	p-value	$\frac{\text{rd}}{\text{df}}$	AIC	n
2021001 – SC	0.033	< 0.001	319.454	32118	102
2020092 – SC	0.179	< 0.001	199.678	20141	102
2020214 – SC	0.166	< 0.001	239.728	24146	102
2020306 – SC	0.202	< 0.001	264.762	26649	102
2021001 – SF	0.106	< 0.001	524.521	52625	102
2020092 – SF	0.183	< 0.001	197.639	19937	102
2020214 – SF	0.190	< 0.001	228.603	23033	102
2020306 – SF	0.285	< 0.001	203.564	20529	102
	Study Area 3				
Julians Date	β_1	p-value	$\frac{\text{rd}}{\text{df}}$	AIC	n
2019001 – SC	0.003	< 0.001	1834.626	150697	84
2018091 – SC	0.015	< 0.001	904.238	74406	84
2018213 – SC	0.018	< 0.001	953.281	78427	84
2018305 – SC	0.016	< 0.001	965.863	79459	84
2019001 – SF	0.013	< 0.001	1455.045	119572	84
2018091 – SF	0.015	< 0.001	1216.042	99973	84
2018213 – SF	0.018	< 0.001	1404.663	115440	84
2018305 – SF	0.018	< 0.001	1272.580	104610	84
	Study Area 4				
Julians Date	β_1	p-value	$\frac{\text{rd}}{\text{df}}$	AIC	n
2015001 – SC	0.065	< 0.001	575.735	9275	18
2015091 – SC	0.085	< 0.001	361.929	5854	18
2015213 – SC	0.085	< 0.001	452.918	7310	18
2014305 – SC	0.054	< 0.001	570.406	9190	18
2015001 – SF	0.056	< 0.001	628.882	10125	18
2015091 – SF	0.119	< 0.001	418.934	6766	18
2015213 – SF	0.066	< 0.001	662.745	10667	18
2014305 – SF	0.049	< 0.001	687.544	11064	18

Tab. V *Results from the GL model for the response variable y_2 with different sample sizes 608, 102, 84, and 18 ($\frac{rd}{df}$ – ratio of deviance to degrees of freedom).*

	Study Area 1					
Julians Date	β_1^c	p^c-value	β_1^z	p^z-value	AIC	n
2021001 – SC	0.002	< 0.001	-0.027	< 0.001	14287	608
2020092 – SC	0.003	< 0.001	-0.029	< 0.001	10469	608
2020214 – SC	0.003	< 0.001	-0.027	< 0.001	10111	608
2020306 – SC	0.003	< 0.001	-0.030	< 0.001	11953	608
2021001 – SF	0.005	< 0.001	-0.026	< 0.001	10490	608
2020092 – SF	0.003	< 0.001	-0.028	< 0.001	9208	608
2020214 – SF	0.004	< 0.001	-0.028	< 0.001	8818	608
2020306 – SF	0.005	< 0.001	-0.031	< 0.001	14119	608
	Study Area 2					
Julians Date	β_1^c	p^c-value	β_1^z	p^z-value	AIC	n
2021001 – SC	0.019	< 0.001	-0.110	0.002	308	102
2020092 – SC	0.121	< 0.001	-0.525	< 0.001	238	102
2020214 – SC	0.111	< 0.001	-0.525	< 0.001	242	102
2020306 – SC	0.126	< 0.001	-1.309	0.002	265	102
2021001 – SF	0.063	< 0.001	-0.130	0.001	451	102
2020092 – SF	0.126	< 0.001	-0.496	< 0.001	237	102
2020214 – SF	0.127	< 0.001	-0.556	< 0.001	249	102
2020306 – SF	0.192	< 0.001	-0.593	< 0.001	235	102
	Study Area 3					
Julians Date	β_1^c	p^c-value	β_1^z	p^z-value	AIC	n
2019001 – SC	0.002	< 0.001	-0.009	< 0.001	1023	84
2018091 – SC	0.011	< 0.001	-0.033	< 0.001	542	84
2018213 – SC	0.013	< 0.001	-0.037	< 0.001	572	84
2018305 – SC	0.012	< 0.001	-0.033	< 0.001	615	84
2019001 – SF	0.009	< 0.001	-0.028	< 0.001	843	84
2018091 – SF	0.011	< 0.001	-0.040	< 0.001	713	84
2018213 – SF	0.012	< 0.001	-0.036	< 0.001	806	84
2018305 – SF	0.012	< 0.001	-0.031	< 0.001	889	84
	Study Area 4					
Julians Date	β_1^c	p^c-value	β_1^z	p^z-value	AIC	n
2015001 – SC	-0.001	0.863	-0.244	0.062	88	18
2015091 – SC	0.021	0.026	-0.328	0.071	83	18
2015213 – SC	0.013	0.192	-0.264	0.050	88	18
2014305 – SC	0.008	0.278	-0.29	0.076	87	18
2015001 – SF	0.002	0.803	-0.209	0.099	92	18
2015091 – SF	0.014	0.315	-0.306	0.033	88	18
2015213 – SF	-0.006	0.601	-0.309	0.032	87	18
2014305 – SF	0.002	0.764	-0.552	0.124	88	18

Tab. VI *Results from the ZIP model for the response variable y_1 with different sample sizes 608, 102, 84, and 18 (^{c} – count model, ^{z} – zero-inflation model).*

	Study Area 1					
Julians Date	β_1^c	p^c-value	β_1^z	p^z-value	AIC	n
2021001 – SC	0.003	< 0.001	-0.027	< 0.001	1163191	608
2020092 – SC	0.003	< 0.001	-0.029	< 0.001	834696	608
2020214 – SC	0.004	< 0.001	-0.027	< 0.001	764996	608
2020306 – SC	0.003	< 0.001	-0.030	< 0.001	930256	608
2021001 – SF	0.005	< 0.001	-0.026	< 0.001	805507	608
2020092 – SF	0.003	< 0.001	-0.028	< 0.001	703020	608
2020214 – SF	0.004	< 0.001	-0.028	< 0.001	666013	608
2020306 – SF	0.005	< 0.001	-0.031	< 0.001	1164106	608
	Study Area 2					
Julians Date	β_1^c	p^c-value	β_1^z	p^z-value	AIC	n
2021001 – SC	0.017	< 0.001	-0.111	0.001	10224	102
2020092 – SC	0.107	< 0.001	-0.539	< 0.001	6598	102
2020214 – SC	0.099	< 0.001	-0.531	< 0.001	6949	102
2020306 – SC	0.114	< 0.001	-1.294	0.001	7928	102
2021001 – SF	0.053	< 0.001	-0.130	0.001	16836	102
2020092 – SF	0.111	< 0.001	-0.511	< 0.001	6820	102
2020214 – SF	0.111	< 0.001	-0.567	< 0.001	7760	102
2020306 – SF	0.169	< 0.001	-0.613	< 0.001	6240	102
	Study Area 3					
Julians Date	β_1^c	p^c-value	β_1^z	p^z-value	AIC	n
2019001 – SC	0.002	< 0.001	-0.009	< 0.001	65901	84
2018091 – SC	0.010	< 0.001	-0.033	< 0.001	29418	84
2018213 – SC	0.012	< 0.001	-0.037	< 0.001	32630	84
2018305 – SC	0.011	< 0.001	-0.033	< 0.001	33968	84
2019001 – SF	0.008	< 0.001	-0.028	< 0.001	51664	84
2018091 – SF	0.010	< 0.001	-0.04	< 0.001	40964	84
2018213 – SF	0.011	< 0.001	-0.036	< 0.001	50362	84
2018305 – SF	0.011	< 0.001	-0.031	< 0.001	50798	84
	Study Area 4					
Julians Date	β_1^c	p^c-value	β_1^z	p^z-value	AIC	n
2015001 – SC	0.016	< 0.001	-0.244	0.062	4575	18
2015091 – SC	0.043	< 0.001	-0.328	0.071	3095	18
2015213 – SC	0.036	< 0.001	-0.264	0.05	3740	18
2014305 – SC	0.021	< 0.001	-0.290	0.076	4076	18
2015001 – SF	0.016	< 0.001	-0.209	0.099	4427	18
2015091 – SF	0.050	< 0.001	-0.306	0.033	3845	18
2015213 – SF	0.013	< 0.001	-0.309	0.032	4723	18
2014305 – SF	0.013	< 0.001	-0.552	0.124	4548	18

Tab. VII *Results from the ZIP model for the response variable y_2 with different sample sizes 608, 102, 84, and 18 (^{c} – count model, ^{z} – zero-inflation model).*

criteria (AIC). It can be seen that the AIC values are significantly lower for the ZIP model which indicates that the model fits on the data much better than the GL model.

4. Results and discussion

4.1 Results of correlation analysis

Fig. 3 shows the calculated sample correlation coefficients with their respective p-values for all study areas between the radiance and indicators. All the correlations are positive which in general indicates that the indicator values increase as the radiance increases. The strongest statistically significant correlations were found between the radiance and NSLPs, and the radiance and TNPSLPs for the study areas 1, 2, and 3. Moreover, these correlations are probably slightly higher on average for the radiances at snow-covered condition with the highest value of sample correlation coefficient $r = 0.881$ ($p < 0.001$). However, the correlation coefficients for the study area 4 evince in general appreciably lower correlation values compared to the other ones with the lowest value of correlation coefficient 0.458. The most remarkable decrease in the correlation coefficients was observed in the correlation between the radiance and AMHSLPs. In the case of this relationship, the correlation presents and opposite behaviour with the moderate correlation values for the first three study areas and high correlation values for the study area 4.

According to the calculated correlation values between the radiance and all variables for all study areas, we excluded the AMHSLPs indicator from the subsequent regression analysis due to the moderate correlation values around value 0.5 [30] and low p-values. It is suggested that the radiance could serve as a better proxy for the NSLPs and TNPSLPs than for the AMHSLPs. Therefore, the NSLPs points and TNPSLPs were incorporated into the subsequent regression analysis.

4.2 Results of regression analysis

We used the GL and ZIP models to examine the relationships between the radiance and chosen responses for all study areas and both snow conditions. Results from the GL regression are suffered from the excess zeros and significant overdispersion which can lead to the invalid inference about the significance of estimated beta coefficients due to their underestimated standard errors [40]. Therefore, we included the ZIP model in the analysis that can effectively take into account both issues and can improve the accuracy of the model. To compare both models we used the AIC as we assumed that in the most study areas there are sufficient sample sizes [4]. Values of the AIC resulted from the ZIP regression for all study areas are much better than in the case of the GL regression, and thus the ZIP model indicates better model fit. The estimated values from the ZIP model for β_1s from the count model are nearly positive in all study areas and for both responses and snow conditions. To better interpretation of the estimated coefficients we calculated their incidence rate ratio described mathematically in the following form:

$$IRR_i = e^{\beta_i}. \tag{8}$$

From the estimated coefficients in the count model part (risk group, not always zero) of the ZIP model was found that one unit increase in the radiance can increase the expected rate of the NSLPs in the area by up to 21.17%. A similar maximum increase (18.41%) was indicated also in the relationship between the radiance and TNPSLPs. This was observed in the study area 2. Minimum increase in both responses based on the one unit increase in the radiance was observed in the study area 4. In all study areas, on average, one unit increase in the radiance increases the expected rate of the NSLPs and TNPSLPs by 3.44% and 3.58%, respectively. Estimated coefficients from the zero-inflation part (non-risk group, always zero group) carry negative signs which means that if there is no street-lighting point, and thus zero total nominal power, the incidence of the radiance on the response is substantially less.

5. Conclusions and future work

This paper shows the investigation of the relationships between the NTL data and urban lighting indicators for the local urban areas in the Czech Republic by using the correlation and regression analyses. The sample Pearson correlation coefficients between the radiance for two snow conditions and three selected indicators, the NSLPs, TNPSLPs, and AMHSLPs, at 95% confidence interval were calculated for 4 study areas. NSLPs and TNPSLPs evince strong statistically significant positive correlation with the radiance in the study areas 1, 2, and 3 and moderate correlation in the study area 4 with the correlation coefficients around value of 0.5. Opposite behaviour of correlation values was found between the radiance and AMHSLPs where the moderate correlation values were observed for the study areas 1, 2, and 3 and higher correlation values for the study area 4. The correlation analysis also reveals that the higher values of correlation coefficients are present mostly for radiances at snow-covered condition. One reason that could explain the discrepancy between correlation results for the first three study areas and the fourth is associated with a scale of each study area. This is in accordance what was found by [28].

Subsequently, we turned into inferencing about interpreting statistically significance of the relationships with the use of simple regression analysis. Given that the AMHSLPs generates somewhat lower correlation coefficient values with the radiance nearly in the most study areas, we did not include it into the regression analysis. The regression analysis showed that the ZIP model was a better model than the GL model in terms of AIC. The results obtained from the ZIP model indicate that there is an association between the radiance and urban lighting installations, both in terms of number of the NSLPs and TNPSLPs. From the count model part was observed that the increase in radiance increases values of both responses. On the contrary, the zero-inflation part reveals that no presence of street-lighting points, and thus zero value of total nominal power is associated with substantial less incidence of the radiance.

Our study contributes to the studies of socio-economic activities based on the NTL data at small and medium sized areas. In this paper, we showed that NTL data has positive correlation with the urban lighting installation indicators, in terms of the number of street-lighting points and total nominal power on smaller

and medium scales. Furthermore, with the use of regression analysis it was observed that there is a statistically significant relationship between the radiance and those indicators. However, several limitations and issues in this study should be addressed as follows:

1. Spatial resolution of the NTL composites might be still too coarse to generate better causal explanations by the use of these regression models. NTL data from such coarse spatial resolution produce radiance patterns which can record the NTL radiance contributions from other light sources and not only from street-lighting.

2. The possible presence of clouds in the NTL data can induce a distortion of the upwelling radiance. They can cause substantial drops in the NTL radiance, especially in the presence of thick clouds. Misclassification of clouds is another substantial source of the radiance outliers [44].

3. Operating times of street-lighting installations are not the same from different points of view. For instance, the times of sunset and sunrise are different during different climatic conditions. This is most evident during the winter and summer months. Development of energy saving strategies (turning on/off, dimming) regulating number of luminaire burning hours is another point of view. Therefore, the radiance contribution from street-lighting is time dependent.

4. VIIRS sensor is not able to measure of incoming light in the intense blue "peak" of white LEDs [27]. Thus, the values of radiance can be inaccurate with respect to the fact that, nowadays, in the most cities the high-pressure sodium laps are replaced by the white LEDs.

5. Non-spatial regression analysis that can not accounted for spatial variations of parameters across the space.

Despite these limitations and issues, the present study offers valuable results and perspectives for future work. In future work we would like to study found associations more deeply employing spatial statistics in order to obtain better causal explanations and improve the accuracy of the model.

References

[1] ADDY C.L., WILSON D.K., KIRTLAND K.A., AINSWORTH B.E., SHARPE P., KIMSEY D. Associations of Perceived Social and Physical Environmental Supports With Physical Activity and Walking Behavior. *American Journal of Public Health*. 2004, 94(3), pp. 440–443, doi: 10.2105/AJPH.94.3.440.

[2] BAGAN H., YAMAGATA Y. Analysis of urban growth and estimating population density using satellite images of nighttime lights and land-use and population data. *GIScience & Remote Sensing*. 2015, 52(6), pp. 765–780, doi: 10.1080/15481603.2015.1072400.

[3] BULLOUGH J.D., DONNELL E.T., REA M.S. To illuminate or not to illuminate: Roadway lighting as it affects traffic safety at intersections. *Accident Analysis & Prevention*. 2013, 53, pp. 65–77, doi: https://doi.org/10.1016/j.aap.2012.12.029. ISSN 0001-4575.

[4] CAMPBELL H. The consequences of checking for zero-inflation and overdispersion in the analysis of count data. *Methods in Ecology and Evolution*. 2021, 12(4), pp. 665–680, doi: https://doi.org/10.1111/2041-210X.13559.

[5] CHEN X., NORDHAUS W.D. Using luminosity data as a proxy for economic statistics. *Proceedings of the National Academy of Sciences*. 2011, 108(21), pp. 8589–8594, doi: 10.1073/pnas.1017031108.

[6] CHEN X., NORDHAUS W.D. VIIRS Nighttime Lights in the Estimation of Cross-Sectional and Time-Series GDP. *Remote Sensing*. 2019, 11(9), doi: 10.3390/rs11091057. ISSN 2072-4292.

[7] COESFELD J., KUESTER T., KUECHLY H.U., KYBA C.C.M. Reducing Variability and Removing Natural Light from Nighttime Satellite Imagery: A Case Study Using the VIIRS DNB. *Sensors*. 2020, 20(11), doi: 10.3390/s20113287. ISSN 1424-8220.

[8] DIGITAL MAP–DATA200, ©2010 ČÚZK. *Data200*. 2019. Last visited 2022-09-01. Available also from: https://geoportal.cuzk.cz/(S(rdni1sfafrxh1uxkbqe3s4be))/Default.aspx?lng=EN&mode=TextMeta&side=mapy_data200&text=dSady_mapyData200&head_tab=sekce-02-gp&menu=229.

[9] DONKER S.F., KRUISHEER J., KOOI F., OTHERS. Pedestrian walking speed as a tool to study environment-behavior. 2011.

[10] DUNN P.K., SMYTH G.K. *Generalized Linear Models With Examples in R*. 2018.

[11] ELVIDGE C.D., CINZANO P., PETTIT D.R., ARVESEN J., SUTTON P., SMALL C., NEMANI R., LONGCORE T., RICH C., SAFRAN J., WEEKS J., EBENER S. The Nightsat mission concept. *International Journal of Remote Sensing*. 2007, 28(12), pp. 2645–2670, doi: 10.1080/01431160600981525.

[12] ELVIDGE C.D., BAUGH K.E., ZHIZHIN M.N., HSU F.-C. Why VIIRS data are superior to DMSP for mapping nighttime lights. *Proceedings of the Asia-Pacific Advanced Network*. 2013, 35(0), pp. 62.

[13] ELVIK R. Meta–analysis of evaluations of public lighting as accident countermeasure. *Transportation Research Record*. 1995, 1485(1), pp. 12–24.

[14] FORSYTH D. *Probability and Statistics for Computer Science*. 2017. ISBN 978-3-319-64410-3.

[15] FOTIOS S., YANG B., CHEAL C. Effects of outdoor lighting on judgements of emotion and gaze direction. *Lighting Research & Technology*. 2015, 47(3), pp. 301–315, doi: 10.1177/1477153513510311.

[16] GERBER F., JONG R.D., SCHAEPMAN M.E., SCHAEPMAN-STRUB G., FURRER R. Predicting Missing Values in Spatio-Temporal Remote Sensing Data. *IEEE Transactions on Geoscience and Remote Sensing*. 2018, 56(5), pp. 2841–2853, doi: 10.1109/TGRS.2017.2785240.

[17] GERONIMO R.C., FRANKLIN E.C., BRAINARD R.E., ELVIDGE C.D., SANTOS M.D., VENEGAS R., MORA C. Mapping Fishing Activities and Suitable Fishing Grounds Using Nighttime Satellite Images and Maximum Entropy Modelling. *Remote Sensing*. 2018, 10(10), doi: 10.3390/rs10101604. ISSN 2072-4292.

[18] HU X., QIAN Y., PICKETT S.T.A., ZHOU W. Urban mapping needs up-to-date approaches to provide diverse perspectives of current urbanization: A novel attempt to map urban areas with nighttime light data. *Landscape and Urban Planning*. 2020, 195, pp. 103709, doi: https://doi.org/10.1016/j.landurbplan.2019.103709. ISSN 0169-2046.

[19] HU Y., YAO J. Illuminating economic growth. *Journal of Econometrics*. 2022, 228(2), pp. 359–378, doi: https://doi.org/10.1016/j.jeconom.2021.05.007. ISSN 0304-4076.

[20] IVAN K., HOLOBÁCĂ I.-H., BENEDEK J., TÖRÖK I. VIIRS Nighttime Light Data for Income Estimation at Local Level. *Remote Sensing*. 2020, 12(18), doi: 10.3390/rs12182950. ISSN 2072-4292.

[21] JACKETT M., FRITH W. Quantifying the impact of road lighting on road safety – A New Zealand Study. *IATSS Research*. 2013, 36(2), pp. 139–145, doi: https://doi.org/10.1016/j.iatssr.2012.09.001. ISSN 0386-1112.

[22] JOE H., ZHU R. Generalized Poisson Distribution: the Property of Mixture of Poisson and Comparison with Negative Binomial Distribution. *Biometrical Journal*. 2005, 47(2), pp. 219–229, doi: https://doi.org/10.1002/bimj.200410102.

[23] JOZOVÁ Š., UGLICKICH E., NAGY I., LIKHONINA R. Modeling of discrete questionnaire data with dimension reduction. *Neural Network World*. 2022, 32, pp. 15–41, doi: 10.14311/NNW.2022.32.002. ISSN 1210-0552.

[24] KATZ Y., LEVIN N. Quantifying urban light pollution – A comparison between field measurements and EROS-B imagery. *Remote Sensing of Environment*. 2016, 177, pp. 65–77, doi: https://doi.org/10.1016/j.rse.2016.02.017. ISSN 0034-4257.

[25] LAMBERT D. Zero-Inflated Poisson Regression, with an Application to Defects in Manufacturing. *Technometrics* [online]. 1992, 34(1) [viewed 2023-08-24], pp. 1–14. ISSN 00401706.

[26] L'ECLAIRAGE C.I.D. *Technical Report: A Guide to Urban Lighting Masterplanning*. 2019. Available also from: https://cie.co.at/publications/guide-urban-lighting-masterplanning. ISBN 978-3-902842-16-9.

[27] LEVIN N., KYBA C.C., ZHANG Q., SÁNCHEZ DE MIGUEL A., ROMÁN M.O., LI X., PORTNOV B.A., MOLTHAN A.L., JECHOW A., MILLER S.D., WANG Z., SHRESTHA R.M., ELVIDGE C.D. Remote sensing of night lights: A review and an outlook for the future. *Remote Sensing of Environment*. 2020, 237, pp. 111443, doi: https://doi.org/10.1016/j.rse.2019.111443. ISSN 0034-4257.

[28] LIU C., WANG C., XU Y., CHENGUANG L., LI M., ZHANG D., LIU G., LI W., ZHANG Q., LI Q. Correlation Analysis Between Nighttime Light Data and Socioeconomic Factors on Fine Scales. *IEEE Geoscience and Remote Sensing Letters*. 2022, 19, pp. 1–5, doi: 10.1109/LGRS.2022.3166281.

[29] MARKVICA K., RICHTER G., LENZ G. Impact of urban street lighting on road users' perception of public space and mobility behavior. *Building and Environment*. 2019, 154, pp. 32–43, doi: https://doi.org/10.1016/j.buildenv.2019.03.009. ISSN 0360-1323.

[30] MELLANDER C., LOBO J., STOLARICK K., MATHESON Z. Night-Time Light Data: A Good Proxy Measure for Economic Activity? *PLOS ONE*. 2015, 10(10), pp. 1–18, doi: 10.1371/journal.pone.0139779.

[31] MILLER S.D., STRAKA W., MILLS S.P., ELVIDGE C.D., LEE T.F., SOLBRIG J., WALTHER A., HEIDINGER A.K., WEISS S.C. Illuminating the Capabilities of the Suomi National Polar-Orbiting Partnership (NPP) Visible Infrared Imaging Radiometer Suite (VIIRS) Day/Night Band. *Remote Sensing*. 2013, 5(12), pp. 6717–6766, doi: 10.3390/rs5126717. ISSN 2072-4292.

[32] MURPHY R.E., BARNES W.L., LYAPUSTIN A.I., PRIVETTE J.L., WELSCH C., DELUCCIA F.J., SWENSON H.W., SCHUELER C.F., ARDANUY P.E., KEALY P.M. Using VIIRS to provide data continuity with MODIS. *IGARSS 2001. Scanning the Present and Resolving the Future. Proceedings. IEEE 2001 International Geoscience and Remote Sensing Symposium (Cat. No.01CH37217)*. 2001, 3, pp. 1212–1214 vol.3.

[33] PAINTER K. The influence of street lighting improvements on crime, fear and pedestrian street use, after dark. *Landscape and Urban Planning*. 1996, 35(2), pp. 193–201, doi: https://doi.org/10.1016/0169-2046(96)00311-8. ISSN 0169-2046.

[34] PENA-GARCIA A., HURTADO A., AGUILAR-LUZON M. Impact of public lighting on pedestrians' perception of safety and well-being. *Safety Science*. 2015, 78, pp. 142–148, doi: https://doi.org/10.1016/j.ssci.2015.04.009. ISSN 0925-7535.

[35] PURKRÁBKOVÁ Z., RŮŽIČKA J., BĚLINOVÁ Z., KOREC V. Traffic accident risk classification using neural networks. *Neural Network World*. 2021, 31, pp. 343–353, doi: 10.14311/NNW.2021.31.019. ISSN 1210-0552.

[36] RAZALI N.M., WAH Y.B. Power comparisons of Shapiro-Wilk, Kolmogorov-Smirnov, Lilliefors and Anderson-Darling tests. 2011.

[37] ROMÁN M.O., WANG Z., SHRESTHA R., YAO T., KALB V. *Black Marble User Guide; Version 1.2*. September 2022. Available also from: https://viirsland.gsfc.nasa.gov/Products/NASA/BlackMarble.html.

[38] ROMÁN M.O., WANG Z., SUN Q., KALB V., MILLER S.D., MOLTHAN A., SCHULTZ L., BELL J., STOKES E.C., PANDEY B., SETO K.C., HALL D., ODA T., WOLFE R.E., LIN G., GOLPAYEGANI N., DEVADIGA S., DAVIDSON C., SARKAR S., PRADERAS C., SCHMALTZ J., BOLLER R., STEVENS J., RAMOS GONZÁLEZ O.M., PADILLA E., ALONSO J., DETRÉS Y., ARMSTRONG R., MIRANDA I., CONTE Y., MARRERO N., MACMANUS K., ESCH T., MASUOKA E.J. NASA's Black Marble nighttime lights product suite. *Remote Sensing of Environment*. 2018, 210, pp. 113–143, doi: https://doi.org/10.1016/j.rse.2018.03.017. ISSN 0034-4257.

[39] ROSE C.E., MARTIN S.W., WANNEMUEHLER K., PLIKAYTIS B.D. On the Use of Zero-Inflated and Hurdle Models for Modeling Vaccine Adverse Event Count Data. *Journal of Biopharmaceutical Statistics*. 2006, 16, pp. 463 –481.

[40] SAPUTRO D.R.S., SUSANTI A., PRATIWI N.B.I. The handling of overdispersion on Poisson regression model with the generalized Poisson regression model. *AIP Conference Proceedings*. 2021, 2326(1), pp. 020026, doi: 10.1063/5.0040330. ISSN 0094-243X.

[41] SHARMA R.C., TATEISHI R., HARA K., GHARECHELOU S., IIZUKA K. Global mapping of urban built-up areas of year 2014 by combining MODIS multispectral data with VIIRS nighttime light data. *International Journal of Digital Earth*. 2016, 9(10), pp. 1004–1020, doi: 10.1080/17538947.2016.1168879.

[42] TIAN J., ZHAO N., SAMSON E.L., WANG S. Brightness of Nighttime Lights as a Proxy for Freight Traffic: A Case Study of China. *IEEE Journal of Selected Topics in Applied Earth Observations and Remote Sensing*. 2014, 7(1), pp. 206–212, doi: 10.1109/JSTARS.2013.2258892.

[43] WALUDA C.M., GRIFFITHS H.J., RODHOUSE P.G. Remotely sensed spatial dynamics of the Illex argentinus fishery, Southwest Atlantic. *Fisheries Research*. 2008, 91(2), pp. 196–202, doi: https://doi.org/10.1016/j.fishres.2007.11.027. ISSN 0165-7836.

[44] WANG Z., ROMÁN M.O., KALB V.L., MILLER S.D., ZHANG J., SHRESTHA R.M. Quantifying uncertainties in nighttime light retrievals from Suomi-NPP and NOAA-20 VIIRS Day/Night Band data. *Remote Sensing of Environment*. 2021, 263, pp. 112557, doi: https://doi.org/10.1016/j.rse.2021.112557. ISSN 0034-4257.

[45] WANG Z., SHRESTHA R.M., ROMÁN M.O., KALB V.L. NASA's Black Marble Multiangle Nighttime Lights Temporal Composites. *IEEE Geoscience and Remote Sensing Letters*. 2022, 19, pp. 1–5, doi: 10.1109/LGRS.2022.3176616.

[46] WANVIK P.O. Effects of road lighting: An analysis based on Dutch accident statistics 1987–2006. *Accident Analysis & Prevention*. 2009, 41(1), pp. 123–128, doi: https://doi.org/10.1016/j.aap.2008.10.003. ISSN 0001-4575.

[47] XIE Y., WENG Q. Updating urban extents with nighttime light imagery by using an object-based thresholding method. *Remote Sensing of Environment*. 2016, 187, pp. 1–13, doi: https://doi.org/10.1016/j.rse.2016.10.002. ISSN 0034-4257.

[48] YADAV B., JEYASEELAN L., JEYASEELAN V., DURAIRAJ J., GEORGE S., SELVARAJ K., BANGDIWALA S.I. Can Generalized Poisson model replace any other count data models? An evaluation. *Clinical Epidemiology and Global Health*. 2021, 11, pp. 100774, doi: https://doi.org/10.1016/j.cegh.2021.100774. ISSN 2213-3984.

[49] YANG Z., HARDIN J.W., ADDY C.L. A score test for overdispersion in Poisson regression based on the generalized Poisson-2 model. *Journal of Statistical Planning and Inference*. 2009, 139(4), pp. 1514–1521, doi: https://doi.org/10.1016/j.jspi.2008.08.018. ISSN 0378-3758.

[50] YANG Z., HARDIN J.W., ADDY C.L. Testing overdispersion in the zero-inflated Poisson model. *Journal of Statistical Planning and Inference*. 2009, 139(9), pp. 3340–3353, doi: https://doi.org/10.1016/j.jspi.2009.03.016. ISSN 0378-3758.

[51] YE T., ZHAO N., YANG X., OUYANG Z., LIU X., CHEN Q., HU K., YUE W., QI J., LI Z., JIA P. Improved population mapping for China using remotely sensed and points-of-interest data within a random forests model. *Science of The Total Environment*. 2019, 658, pp. 936–946, doi: https://doi.org/10.1016/j.scitotenv.2018.12.276. ISSN 0048-9697.

[52] ZHAO M., ZHOU Y., LI X., CAO W., HE C., YU B., LI X., ELVIDGE C.D., CHENG W., ZHOU C. Applications of Satellite Remote Sensing of Nighttime Light Observations: Advances, Challenges, and Perspectives. *Remote Sensing*. 2019, 11(17), doi: 10.3390/rs11171971. ISSN 2072-4292.

[53] ZHAO N., HSU F.-C., CAO G., SAMSON E.L. Improving accuracy of economic estimations with VIIRS DNB image products. *International Journal of Remote Sensing*. 2017, 38(21), pp. 5899–5918, doi: 10.1080/01431161.2017.1331060.